Comparison of Models for the Prediction of Hydrodynamic Parameters in Structured Packing Columns for Biogas Purification

Hamadi CHERIF*, Christophe COQUELET*, Paolo STRINGARI*‡, Denis CLODIC**, Joseph TOUBASSY**

* CTP - Centre of Thermodynamics of Processes, MINES Paris Tech, PSL Research University, 35 rue St Honoré 77305 Fontainebleau, France

** Cryo Pur R&D society, 3 Rue de la croix martre, 91120 Palaiseau, France

(hamadi.cherif@mines-paristech.fr, christophe.coquelet@mines-paristech.fr, paolo.strinagri@mines-paristech.fr, denis.clodic@cryopur.com, joseph.toubassy@cryopur.com)

‡ Corresponding Author; Paolo STRINGARI, 35 rue St Honoré 77305 Fontainebleau, France, Tel: +33 1 64 69 48 57,

paolo.stringari@mines-paristech.fr

Abstract- This work compares three existing models used for the prediction of hydrodynamic parameters in structured packing columns. These models are used to evaluate pressure drop, liquid holdup, effective interfacial area, mass transfer coefficients and transition points. The results obtained with these models are compared to experimental data in order to choose the one with the best fit. Comparisons were made using Flexipac 350Y structured packing and two systems: Air – Water and Air – Kerosol 200. The model chosen is based on semi-empirical correlations using constants and exponents defined according to experimental measurements. To adapt the model to biogas application and to make it more representative of the system of interest, these constants were optimised and some exponents have been adjusted. Once the model modified, the results of pressure drop were compared to data from an industrial pilot plant treating 85 Nm^3/h of biogas which contains about 30 ppm of hydrogen sulfide (H$_2$S) treated in a structured packing column.

Keywords Hydrodynamics, Structured packing, Pressure drop, Liquid holdup, Effective interfacial area.

1. Introduction

Absorption technology is widely used in natural gas industry to remove water and / or acid gases. Application of the principle of absorption is based on contacting the gas and the liquid phases in a gas-liquid contactor called absorber.

There are a large number of gas-liquid contactors used in industry for heat and mass transfer between the two phases. The choice of the absorber is mainly related to the physicochemical properties of the gas to be treated and to the chemical reactions involved, as well as implemented gas and liquid flow rates. Generally, a counter current two-phase flow is employed to achieve significant concentration gradients and better absorption rate and the absorbers are usually equipped with internal devices to generate the largest interfacial area for a better mass exchange between the two phases in contact.

In prior years, plate columns were heavily favoured over packed columns. But, nowadays these latter are the most used in gas absorption applications. Only few specific applications with special design requirements can lead to different choices such as in the case of very large flow rates or very soluble compounds where it is preferable to use plate or spray columns.

In a packed column, the gas and liquid normally flow counter currently as seen in Fig. 1. The liquid is injected from the top of the column to flow by gravity on the packing forming a large-area liquid film. The liquid is contacted with the gas injected from the bottom of the column. Liquid flow must be sufficient to ensure uniform wetting of the packing

and must not exceed a certain threshold in order to avoid flooding of the column. The selection of the packing type and material is a very important issue in packed column design. The material should respect certain requirements as weight, pressure drop and especially corrosion resistance.
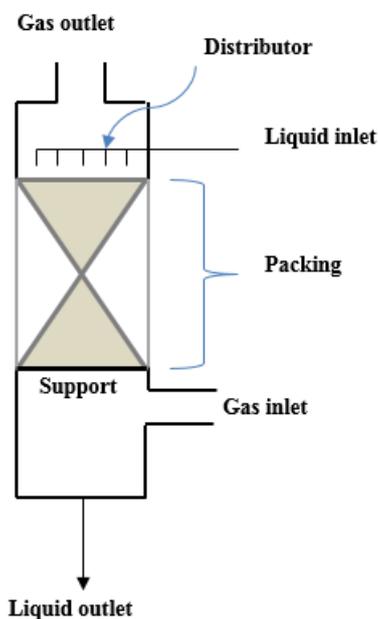

Fig. 1. Schematic representation of a packing column.

There exist two types of packing: those consisting of packing elements placed in a random disposition and those containing corrugated sheets arranged in an orderly manner. The first one is called random packing and the latter is called structured packing.

Today, in modern absorption columns, structured packings are widely used, thanks to their higher capacity and lower pressure drop compared to random packings. Structured packings were used for the first time in 1950 [1]. They are in continuous development to expand their use and improve their efficiency. They provide a large surface area for the liquid and gas phases to be in direct contact within the column. High efficient mass transfer between the two phases is achieved thanks to the packing surface.

2. Experiments

Experiments were performed on the industrial demonstrator "BioGNVAL" treating 85 Nm³/h of biogas from the Valenton wastewater treatment plant, the second biggest in France run by the SIAAP (Public society serving the Paris region). The demonstrator developed by the company Cryo Pur® was built in partnership with SUEZ as part of the BioGNVAL project, and partially funded by the 'Invest in the Future' program run by the ADEME (French Environment and Energy Management Agency). GNVert (Engie) and IVECO are also partners in the BioGNVAL project, providing the Bio-LNG distribution station and the heavy goods vehicle Flex Fuel gas / Bio-LNG respectively.

The BioGNVAL pilot plant, shown in Fig. 2, uses a cryogenic technology to upgrade and liquefy biogas efficiently without loss of methane and without emitting greenhouse gases. The system generates two products from biogas: liquid bio-methane and bioCO₂ at purity level greater than 99.995 % respecting EIGA (European Industrial Gases Association) specifications [2].

The type of packing used in experiments is Montz® with a specific geometric packing surface area of 420 m²/m³. The packing column is placed upstream of the process in order to eliminate H_2S from biogas using an aqueous solution of sodium hydroxide.

Fig. 2. BioGNVAL demonstrator located at Valenton wastewater treatment plant.

3. Theoretical principles

In a packed column, hydrodynamics and mass transfer processes occur simultaneously. They are correlated and the link parameter is liquid holdup h_L defined as the volume of the liquid per unit volume of the column. Eq. (1) defined by Chan and Fair [4] for sieve trays illustrated the relation between the two processes.

$$k_V a_e = \frac{316 \, D_V^{0,5} \, (1030 \, f + 867 \, f^2)}{h_L^{0,5}} \qquad (1)$$

Where k_V is the gas phase mass transfer coefficient, a_e is the effective interfacial area, D_V is the gas phase diffusion coefficient, f is the approach to flood.

Regarding the hydrodynamic analysis, increasing the velocity of liquid and gas results in an increase of the liquid holdup and the thickness of the liquid film, which leads to an increase in pressure drop.

About mass transfer analysis, increasing liquid holdup causes the enlargement of the interfacial area leading to higher mass transfer rates.

The curve which represents the evolution of the pressure drop or the liquid holdup as a function of the gas capacity factor F_c is divided by two points (loading and flooding points) into three operating regions as seen in Fig. 3.

$$F_c = u_V \times \sqrt{\rho_V} \qquad (2)$$

Where u_V is the superficial gas velocity and ρ_V is the density of the gas phase.

The loading point represented by the line AA in Fig. 3 is reached when the slope of the liquid holdup curve starts to increase, or when the wet pressure drop curve starts to deviate from the pressure drop in a dry column.

The flooding point is represented by the line BB in Fig. 3. It is the point where the slope of pressure drop and liquid holdup curves tends toward infinity.

Therefore, it is necessary to predict accurately the transition points because they characterize the capacity of a packing column. According to Paquet [5], under-predicting the flooding point will prevent the column to operate at its optimal conditions and its capacity could be very low. However, over-predicting the flooding point may lead to higher pressure drop which could be problematic.

Because of the lack of predictive models, and because of the imprecision of existing ones to accurately predict the hydrodynamic parameters for some specific applications such as biogas purification, most distillation and packing columns are still being designed based on experimental data from a pilot plant [6].
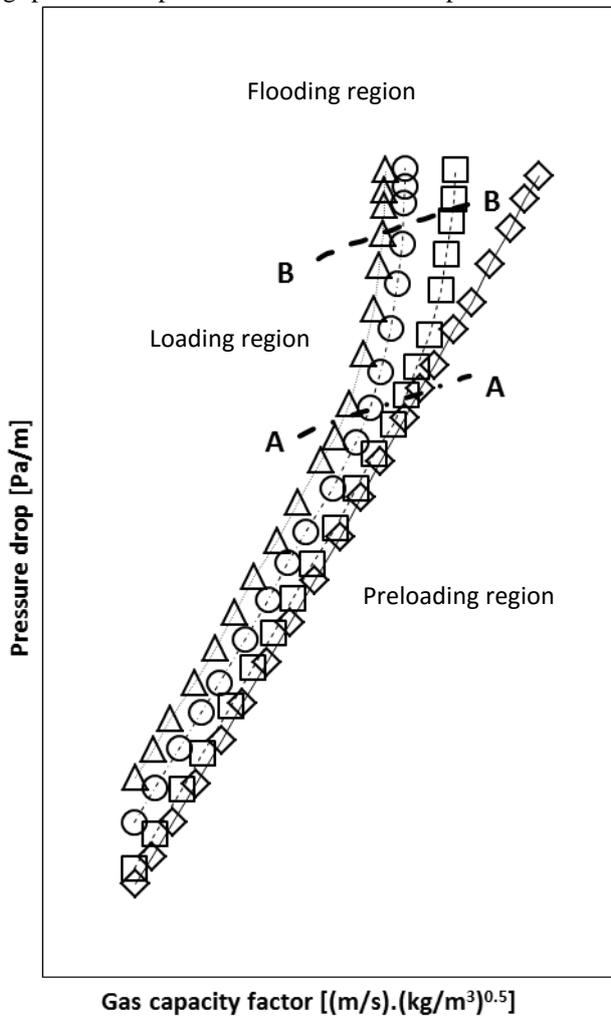

Fig. 3a. Pressure drop evolution in a packing column.

(—Δ—) Dry bed ; (- -□- -) 1 ; (- ·○- ·) 2 ; (···Δ···) 3
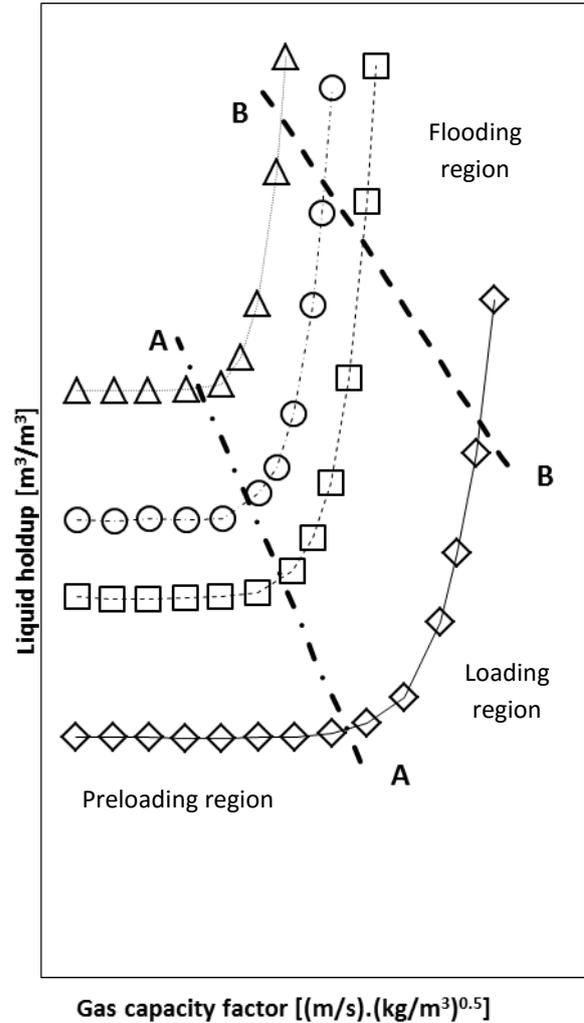(AA) Loading point ; (BB) Flooding point
Liquid load: 1 < 2 < 3

Fig. 3b. Liquid holdup evolution in a packing column.

(—Δ—) 1 ; (- -□- -) 2 ; (- ·○- ·) 3 ; (···Δ···) 4
(AA) Loading point ; (BB) Flooding point
Liquid load: 1 < 2 < 3 < 4

The objective of this work is to find a model adapted for the representation of the experimental results obtained on the BioGNVAL pilot plant. To this aim, three literature models for the hydrodynamics in structured packing columns have been compared: Billet and Schultes [7], SRP [8] and Delft models [9].

These models have been developed on dimensionless analysis and experimental data obtained using a distillation column. The two first models are implemented in the process simulator Aspen Plus®. The three models are described in detail in the following section.

3.1. Billet and Schultes model

The Billet and Schultes model [7] was at the base founded for random packings. Then, it was extended to cover structured packings. Based on semi-empirical

correlations, this model assumes that the packing void fraction ε is represented by vertical tubes where the liquid is sprayed from the top as a film that meets the gas flow in a counter-current configuration. The angle between the corrugations of the packing θ is not taken into account by the Billet and Schultes model.

As reported by Paquet [5], the main disadvantage of this model is that it requires six specific constants for each type of packing. The ones needed for Flexipac 350Y are presented in Table 1.

Table 1. Flexipac 350Y constants for the Billet and Schultes model

Manufacture	Material	Description	a (m^2/m^3)	ε	C_{lp}	C_{Fl}	C_h	C_p	C_L	C_V
Flexipac	Metal	350Y	350	0.985	3.157	2.464	0.482	0.172	1.165	0.422

Where a is the specific geometric packing area, C_{lp} is the specific packing constant for calculation of hydrodynamic parameters at loading point, C_{Fl} is the specific packing constant for calculation of hydrodynamic parameters at flooding point, C_h is the specific packing constant for hydraulic area, C_p is the specific packing constant for pressure drop calculation, C_L is the specific packing constant for mass transfer calculation in liquid phase, C_V is the specific packing constant for mass transfer calculation in gas phase.

Correlations (3), (4) and (5) illustrated in Table 2 are used by Billet and Schultes to calculate the effective interfacial area at loading point, in the loading region and at the flooding point respectively.

Table 2. Effective interfacial area in packing columns using Billet and Schultes model [10]

Parameter	Correlation	
Effective interfacial area at loading point	$$\left(\frac{a_\varepsilon}{a}\right)_{lp} = 1.5\,(a\,d_h)^{-0.5}\left(\frac{u_L\,d_h}{\nu_L}\right)^{-0.2}\left(\frac{u_L^2\,\rho_L\,d_h}{\sigma_L}\right)^{0.75}\left(\frac{u_L^2}{g\,d_h}\right)^{-0.45}$$ $$= 1.5\,(a\,d_h)^{-0.5}\quad Re_L^{-0.2}\quad We_L^{0.75}\quad Fr_L^{-0.45}$$	(3)
Effective interfacial area in loading region	$$\left(\frac{a_e}{a}\right)_{u_V>u_{V,lp}} = \left(\frac{a_e}{a}\right)_{lp} + \left[\left(\frac{a_e}{a}\right)_{Fl} - \left(\frac{a_e}{a}\right)_{lp}\right]\left(\frac{u_{V,lp}}{u_{V,Fl}}\right)^{13}$$	(4)
Effective interfacial area at flooding point	$$\left(\frac{a_\varepsilon}{a}\right)_{Fl} = 7\left(\frac{\sigma_L}{\sigma_W}\right)^{0.56}\left(\frac{a_\varepsilon}{a}\right)_{lp}$$	(5)

Where d_h is the hydraulic diameter, u_L is superficial liquid velocity, ν_L is the kinematic viscosity of the liquid phase, ρ_L is the liquid density, σ_L and σ_W are the surface tension of the liquid phase and water respectively, g is the gravitational constant, Re_L is the liquid Reynolds number, We_L is the liquid Weber number and Fr_L is the liquid Froude number.

The Billet and Schultes model is composed of several correlations that describe liquid holdup and pressure drop in the preloading, loading and flooding regions. Velocities and liquid holdup at loading and flooding points are calculated using the equations listed in Tables 3.

Table 3. Liquid holdup and velocities at loading and flooding points [11]

Parameter	Correlation	
Gas velocity at loading point	$$u_{V,lp} = \sqrt{\frac{g}{\psi_{lp}}}\left(\frac{\varepsilon}{a^{\frac{1}{6}}} - a^{0.5}\left(\frac{12}{g}\frac{\mu_L}{\rho_L}u_{L,lp}\right)^{\frac{1}{3}}\right)\left(\frac{12}{g}\frac{\mu_L}{\rho_L}u_{L,lp}\right)^{\frac{1}{6}}\sqrt{\frac{\rho_L}{\rho_V}}$$	(6)
Liquid velocity at loading point	$$u_{L,lp} = \frac{\rho_V}{\rho_L}\frac{L}{V}u_{V,lp}$$	(7)
Gas velocity at flooding point	$$u_{V,Fl} = \sqrt{\frac{2g}{\psi_{Fl}}\frac{(\varepsilon - h_{L,Fl})^{\frac{3}{2}}}{\varepsilon^{0.5}}} - \sqrt{\frac{h_{L,Fl}}{a}}\sqrt{\frac{\rho_L}{\rho_V}}$$	(8)

Resistance coefficient at loading point	$$\psi_{lp} = \frac{g}{C_{lp}^2 \left(\frac{L}{V}\sqrt{\frac{\rho_V}{\rho_L}}\left(\frac{\mu_L}{\mu_V}\right)^{0.4}\right)^{2n_{lp}}}$$	(9)
Resistance coefficient at flooding point	$$\psi_{Fl} = \frac{g}{C_{Fl}^2 \left(\frac{L}{V}\sqrt{\frac{\rho_V}{\rho_L}}\left(\frac{\mu_L}{\mu_V}\right)^{0.2}\right)^{2n_{Fl}}}$$	(10)
Packing specific constant at loading point	$$\frac{L}{V}\sqrt{\frac{\rho_V}{\rho_L}} \leq 0.4 \rightarrow n_{lp} = -0.326 \rightarrow C_{lp} = C_{lp}$$ $$\frac{L}{V}\sqrt{\frac{\rho_V}{\rho_L}} > 0.4 \rightarrow n_{lp} = -0.723 \rightarrow C_{lp} = 0.695\, C_{lp}\left(\frac{\mu_L}{\mu_V}\right)^{0.1588}$$	(11)
Packing specific constant at flooding point	$$\frac{L}{V}\sqrt{\frac{\rho_V}{\rho_L}} \leq 0.4 \rightarrow n_{Fl} = -0.194 \rightarrow C_{Fl} = C_{Fl}$$ $$\frac{L}{V}\sqrt{\frac{\rho_V}{\rho_L}} > 0.4 \rightarrow n_{Fl} = -0.708 \rightarrow C_{Fl} = 0.6244\, C_{Fl}\left(\frac{\mu_L}{\mu_V}\right)^{0.1028}$$	(12)
Liquid holdup at the loading point	$$h_{L,lp} = \left(\frac{12\, a^2\, \mu_L\, u_L}{\rho_L\, g}\right)^{\frac{1}{3}}$$	(13)
Liquid holdup at the flooding point	$$h_{L,Fl}^3\left(3h_{L,Fl} - \varepsilon\right) = \frac{6}{g}\, a^2\, \varepsilon\, \frac{\mu_L}{\rho_L}\, \frac{L}{V}\, \frac{\rho_V}{\rho_L}\, u_{V,Fl}$$	(14)

Where ψ is the resistance coefficient, μ is the dynamic viscosity, L and V are the liquid and gas flow rates respectively, n is an exponent for calculation of liquid holdup.

Table 4 presents the correlations used by Billet and Schultes to calculate the liquid holdup in the loading region. This property depends on the liquid holdup in the preloading region and at the flooding point. The first one is theoretically derived from a force balance, while the second is purely empirical.

The liquid holdup in the preloading region does not depend on the gas properties. It is only a function of the liquid properties and its velocity, as seen in Eq. (15).

As stated in the thesis of Paquet [5], the hydraulic area of the packing accounts for the surfaces that were not completely wetted by the liquid flow.

Table 4. Liquid holdup in preloading and loading regions [10]

Parameter	Correlation	
Liquid holdup in preloading region	$$h_{L,pl} = \left(12\, \frac{\mu_L\, a^2\, u_L}{\rho_L\, g}\right)^{\frac{1}{3}}\left(\frac{a_h}{a}\right)^{\frac{2}{3}}$$	(15)
Hydraulic area of the packing	$$\frac{a_h}{a} = C_h\, Re_L^{0.15}\, Fr_L^{0.1} \qquad For\ Re_L < 5$$ $$\frac{a_h}{a} = 0.85\, C_h\, Re_L^{0.25}\, Fr_L^{0.1} \qquad For\ Re_L \geq 5$$	(16)
Liquid Reynolds number	$$Re_L = \frac{u_L \rho_L}{a\, \mu_L}$$	(17)

Liquid Froude number	$Fr_L = \dfrac{u_L^2\, a}{g}$	(18)
Liquid holdup at flooding point	$h_{L,Fl} = 2.2\, h_{L,pl}$	(19)
Liquid holdup in loading region	$h_L = h_{L,pl} + \left(h_{L,Fl} - h_{L,pl}\right)\left(\dfrac{u_V}{u_{V,Fl}}\right)^{13}$	(20)

The equations used to calculate pressure drop are listed in Table 5.

Table 5. Liquid holdup in preloading and loading regions [10]

Parameter	Correlation	
Dry pressure drop	$\left(\dfrac{dP}{dz}\right)_d = \psi_0\, \dfrac{a}{\varepsilon^3}\, \dfrac{F_c^2}{2}\, \dfrac{1}{K}$	(21)
Resistance coefficient	$\psi_0 = C_p\left(\dfrac{64}{Re_V} + \dfrac{1.8}{Re_V^{0.08}}\right)$	(22)
Gas capacity factor	$F_c = u_V\sqrt{\rho_V}$	(23)
Wall factor	$\dfrac{1}{K} = 1 + \dfrac{2}{3}\, \dfrac{1}{(1-\varepsilon)}\, \dfrac{d_p}{d}$	(24)
Particle diameter	$d_p = 6\, \dfrac{1-\varepsilon}{a}$	(25)
Gas Reynolds number	$Re_V = \dfrac{u_V\, d_p\, \rho_V}{(1-\varepsilon)\, \mu_V}\, K$	(26)
Wet pressure drop	$\dfrac{dP}{dz} = \psi_L\, \dfrac{f_w\, a}{(\varepsilon - h_L)^3}\, \dfrac{F_c^2}{2}\, \dfrac{1}{K}$	(27)
Resistance factor	$\psi_L' = \psi_L\, f_w = C_p\, f_s\left(\dfrac{64}{Re_V} + \dfrac{1.8}{Re_V^{0.08}}\right)\left(\dfrac{\varepsilon - h_L}{\varepsilon}\right)^{(1.5)}$	(28)
f_s	$f(s) = \left(\dfrac{h_L}{h_{L,lp}}\right)^{0.3} \exp\left(\dfrac{Re_L}{200}\right)$	(29)

The expression of dry pressure drop (Eq. 21) is obtained by applying a force balance. The wall factor K is used to take into account the free spaces more available at the wall. The constant C_p used to calculate the resistance coefficient ψ_0 characterizes the geometry of the packing.

For the wetted packing column, Eq. (27) used to calculate pressure drop replaces the void fraction (ε) by an effective void fraction ($\varepsilon - h_L$) which depends on liquid holdup reducing the volume available for the gas flow. This equation introduces a wetting factor f_w to account for any change in the surface of the packing caused by the wetting action [5].

3.2. SRP model

The SRP (Separations Research Program) model [8] was developed at the University of Texas [12]. The latest version of this model was published in the work of Bravo et al. in 2000 [8].
According to Paquet [5], the SRP model considers the void fraction as a series of wet columns where the gas flow passes through. Unlike the Billet and Schultes model, the packing geometry depends on the angle and dimensions of corrugations.

To calculate liquid holdup and effective interfacial area, the SRP model uses a correction factor that takes into account the packing surface that is not completely wetted by the liquid flow.

The prediction of the effective interfacial area is based on a simple equation that depends on the liquid holdup correction factor and a surface enhancement factor as seen in Table 6. The surface enhancement factor is equal to 0.35 for stainless steel sheet metal packing [12].

Table 6. Effective interfacial area in packing columns using SRP model [8]

Parameter	Correlation	
Liquid Reynolds number	$$Re_L = \frac{s\, u_L\, \rho_L}{\mu_L}$$	(30)
Liquid Froude number	$$Fr_L = \frac{u_L^2}{s\, g}$$	(31)
Liquid Weber number	$$We_L = \frac{s\, \rho_L\, u_L^2}{g\, \sigma_L}$$	(32)
Solid – liquid film contact angle	For $\sigma_L \leq 0{,}055\ N.m^{-1}$ $\quad cos\gamma = 0{,}9$ For $\sigma_L > 0{,}055\ N.m^{-1}$ $\quad cos\gamma = 5{,}211 \times 10^{-16{,}835\ \sigma_L}$	(33)
Correction factor	$$F_t = \frac{29{,}12\, s^{0{,}359}\, (We_L\, Fr_L)^{0{,}15}}{\varepsilon^{0{,}6}\, Re_L^{0{,}2}\, (sin\theta)^{0{,}3}\, (1 - 0{,}93\, cos\gamma)}$$	(34)
Effective interfacial area	$$\frac{a_e}{a} = F_t\, F_{SE}$$	(35)

The SRP model uses the effective gravity which takes into account forces that oppose the flow of the liquid film over the packing. These forces are caused by the pressure gradient, buoyancy and shear stress in the gas phase [5].

An iterative approach exploiting this effective gravity is used to calculate liquid holdup. The calculation steps followed for predicting liquid holdup in a packing column are shown in Table 7.

Table 7. Liquid holdup in packing column using SRP model [8]

Parameter	Correlation	
Dry pressure drop	$$\left(\frac{\Delta P}{\Delta z}\right)_d = \frac{A\, \rho_V}{s\, \varepsilon^2\, (sin\theta)^2}\, u_V^2 + \frac{B\, \mu_V}{s^2\, \varepsilon\, sin\theta}\, u_V$$	(36)
Initial condition for the iterative approach	$$\left(\frac{\Delta P}{\Delta z}\right)_{iter} = \left(\frac{\Delta P}{\Delta z}\right)_d$$	(37)
Iterative approach	$$h_L = \left(\frac{4\, F_t}{s}\right)^{\frac{2}{3}} \left[\frac{3\, \mu_L\, u_L}{\rho_L\, \varepsilon\, g_{eff}\, sin\theta}\right]^{\frac{1}{3}}$$ $$\frac{\Delta P}{\Delta z} = \frac{\left(\frac{\Delta P}{\Delta z}\right)_d}{[1 - h_L(71{,}35\, s + 0{,}614)]^5}$$	(38)
Convergence	$$If\ \frac{\Delta P}{\Delta z} \neq \left(\frac{\Delta P}{\Delta z}\right)_{iter} \rightarrow \left(\frac{\Delta P}{\Delta z}\right)_{iter} = \frac{\Delta P}{\Delta z}\ and\ restart\ from\ (37)$$ $$If\ \frac{\Delta P}{\Delta z} \approx \left(\frac{\Delta P}{\Delta z}\right)_{iter} \rightarrow Convergence$$	(39)

The constants A and B used to calculate the pressure drop in a dry column depend on the type of the packing. For metal structured packings, A and B are equal to 0.177

and 88.77 respectively [13]. Table 8 presents the equations used for the prediction of pressure drop in preloading and loading regions.

Table 8. Pressure drop in packing column using SRP model [8]

Parameter	Correlation	
Liquid film thickness	$$\delta = \left(\frac{3\ \mu_L\ u_L}{a\ g\ \rho_L\ sin\theta} \right)^{\frac{1}{3}}$$	(40)
Gas flow channel diameter	$$d_{hV} = \frac{\frac{(b\ h - 2\ s\ \delta\ )^2}{b\ h}}{\left[\left(\frac{b\ h - 2\ s\ \delta}{2\ h} \right)^2 + \left(\frac{b\ h - 2\ s\ \delta}{b} \right)^2 \right]^{0,5} + \frac{b\ h - 2\ s\ \delta}{2\ h}}$$	(41)
Gas capacity factor at loading point	$$F_{c,lp} = \left[0,053\ g\ d_{hV}\ \varepsilon^2\ (sin\theta)^{1,15}\ (\rho_L - \rho_V) \left(\frac{u_L}{u_V} \sqrt{\frac{\rho_L}{\rho_V}} \right)^{-0,25} \right]^{0,5}$$	(42)
Pressure drop enhancement factor	$$F_l = 3,8 \left(\frac{F_c}{F_{c,lp}} \right)^{\frac{2}{sin\theta}} \left(\frac{u_L^2}{g\ d_{hV}\ \varepsilon^2} \right)^{0,13}$$	(43)
Pressure drop in preloading region	$$\left(\frac{\Delta P}{\Delta z} \right)_{pl} = \left(\frac{\Delta P}{\Delta z} \right)_d \left(\frac{1}{[1 - h_L(71,35\ s + 0,614)]} \right)$$	(44)
Pressure drop in loading region	$$\left(\frac{\Delta P}{\Delta z} \right) = F_l \left(\frac{\Delta P}{\Delta z} \right)_{pl}$$	(45)

3.3. Delft model

The Delft model [9] was developed in a joint academic project between Montz Company and Delft University of Technology. The Delft model considers that all the packing surface area is wetted by the liquid film [5]. The prediction of the effective interfacial area with the Delft model is based on an empirical correlation presented in Eq. (46).

$$a_e = a\ \frac{(1 - \Omega)}{\left(1 + \frac{A}{u_L^B} \right)} \tag{46}$$

According to Paquet [5], Ω is equal to 0.1 for Montz Packing and for most packing with holes as Flexipac and Mellapak. A and B are constants specific to the type and size of the packing. For example, these two constants are respectively equal to 2.143 x 10^-6 and 1.5 for Montz Packing B1-250 [12].

The Delft model introduces a new expression to define the effective liquid flow angle as seen in Eq. (47).

$$\alpha_L = arctan \left[\frac{cos\ (90 - \theta)}{sin\ (90 - \theta)\ cos \left[arctan \left(\frac{b}{2\ h} \right) \right]} \right] \tag{47}$$

This model uses a simple function for predicting liquid holdup consisting on the product of the specific surface of the packing and the thickness of the liquid film.

$$h_L = \delta\ a \tag{48}$$

The expression of the liquid film thickness is the same adapted by the SRP model except that it uses the effective liquid flow angle.

For the prediction of the pressure drop, the Delft model uses the same equations as the SRP model. The only difference is situated in the preloading region. As reported by Paquet [5], the Delft model assumes that the gas flows in a regular zigzag pattern through the packed column. It uses three parameters which contribute to the calculation of the pressure drop in the preloading region.
The details of calculation of pressure drop in the preloading region are summarized in Table 9.

Table 9. Pressure drop in preloading region using Delft model [8]

Parameter	Correlation	
Effective gas velocity	$$u_{V,e} = \frac{u_V}{\varepsilon\,(1 - h_L)\,\sin\theta}$$	(49)
Effective liquid velocity	$$u_{L,e} = \frac{u_L}{h_L\,\varepsilon\,\sin\alpha_L}$$	(50)
Relative Reynolds number for gas phase	$$Re_{Vr} = \frac{\rho_V\,d_{hV}\,(u_{V,e} + u_{L,e})}{\mu_V}$$	(51)
Effective Reynolds number for gas phase	$$Re_{Ve} = \frac{\rho_V\,d_{hV}\,u_{V,e}}{\mu_V}$$	(52)
Fraction of the flow channel occupied by the liquid phase	$$\varphi = \frac{2\,s}{2\,s + b}$$	(53)
Fraction of the channels ending at the column wall	$$\psi = \frac{2}{\Pi}\,arcsin\left(\frac{h_{pe}}{d_c\,\tan\theta}\right) + \frac{2\,h_{pe}}{\Pi\,d_c^2\,\tan\theta}\left(d_c^2 - \frac{h_{pe}^2}{\tan^2\theta}\right)^{0,5}$$	(54)
Gas/Liquid friction coefficient	$$\xi_{GL} = \left[-2\,log_{10}\left[\frac{\delta}{3,7\,d_{hV}} - \frac{5,02}{Re_{Vr}}\,log_{10}\left(\frac{\delta}{3,7\,d_{hV}} + \frac{14,5}{Re_{Vr}}\right)\right]\right]^{-2}$$	(55)
Gas/Gas friction coefficient	$$\xi_{GG} = 0,722\,(cos\theta)^{3,14}$$	(56)
Direction change coefficient in the bulk zone	$$\xi_{bulk} = 1,76\,(cos\theta)^{1,63}$$	(57)
Direction change coefficient for wall zone	$$\xi_{wall} = 34,19\,u_L^{0,44}\,(cos\theta)^{0,779} + \frac{4092\,u_L^{0,31} + 4715\,(cos\theta)^{0,445}}{Re_{Ve}}$$	(58)
Coefficient for gas/liquid friction losses	$$\varsigma_{GL} = \xi_{GL}\,\varphi\,\frac{h_{pb}}{d_{hV}\,\sin\theta}$$	(59)
Coefficient for gas/gas friction losses	$$\varsigma_{GG} = \xi_{GG}\,\frac{h_{pb}}{d_{hV}\,\sin\theta}\,(1 - \varphi)$$	(60)
Coefficient for losses caused by direction change	$$\varsigma_{DC} = \frac{h_{pb}}{h_{pe}}\,(\xi_{bulk} + \psi\,\xi_{wall})$$	(61)
Pressure drop in preloading region	$$\Delta P_{pl} = \Delta P_{GG} + \Delta P_{GL} + \Delta P_{DC} = \frac{1}{2}\,\rho_V u_{V,e}^2\,(\varsigma_{GG} + \varsigma_{GL} + \varsigma_{DC})$$	(62)

4. Models Evaluation

The three models introduced in the previous section are evaluated and compared in order to choose the most effective in the prediction of hydrodynamic properties. To achieve this, the models are compared using two systems: Air / Water and Air / Kerosol 200. These systems have been chosen because of the lack of experimental data in the open literature concerning the system of interest (biogas with H_2S / aqueous solution of sodium hydroxide).

Kerosol is a paraffin characterized by a low surface tension and high viscosity as seen in Table 10. "200" refers to its boiling point (200 °C).

The differences in liquid surface tension, density and viscosity between water and Kerosol 200 allow comparison of models for different conditions, highlighting the effects on pressure drop and liquid holdup.

The experimental data were retrieved from the work of Erasmus [12].

Table 10. Physical properties of the systems tested [12]

Component	Density [kg/m^3]	Viscosity [kg/m.s]	Surface tension [N/m]
Air	0.81	18.10^{-6}	-
Water	1000	0.001	71.2 x 10^{-3}
Kerosol 200	763	2.31 x 10^{-3}	23.9 x 10^{-3}

The type of packing used for this comparison is Flexipac 350Y. This packing is different with respect to the one used in the BioGNVAL pilot plant (Montz B1-420), but no literature data are available for this last. The dimensions of Flexipac 350Y are outlined in Table 11 and the relative constants used by Billet and Schultes are shown in Table 1.

Table 11. Dimensions of Flexipac 350Y [12]

Property	Value
Void fraction	0.985
Corrugation angle	45 °
Corrugation base	15.5 mm
Corrugation side	11.5 mm
Crimp height	8.4 mm
Height of element	265 mm

4.1. Pressure drop and liquid holdup

In Fig. 4, the experimentally determined pressure drop and liquid holdup over Flexipac 350Y [12] are compared to the results obtained with the models using an Air – Water system.

Fig. 4a shows that SRP and Billet and Schultes models are accurate in predicting the pressure drop in preloading region (F_c < 1.9). The Delft model predicts the correct shape of the pressure drop curve, but compared to the experimental data, the results obtained are not realistic.
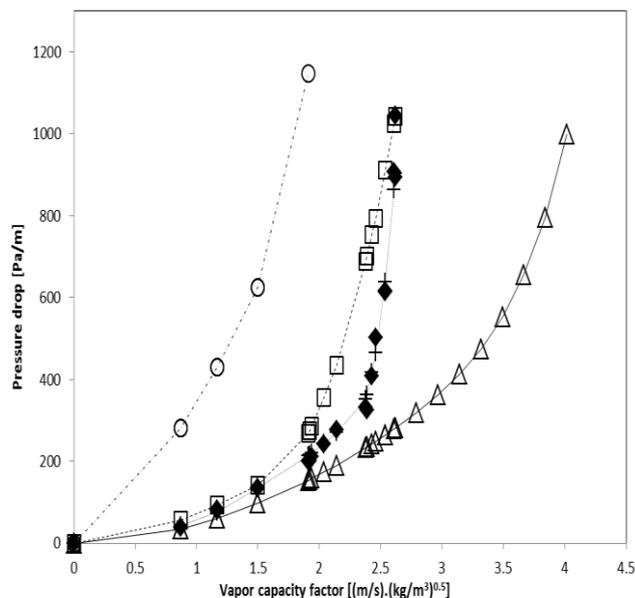

Fig. 4a. Pressure drop evaluation for liquid load u_L = 20.5 m/h.

Models: (—△—) Billet & Schultes ; (- -□- -) SRP ; (- ·○- ·) Delft ; (···+···) Billet & Schultes modified "Section 5" ; Experimental values: (♦) [12]

Although the results are not accurate, Fig. 4b shows that the model by Billet and Schultes is the best in predicting liquid holdup in a structured packed column. The Delft model assumes that the liquid holdup is not influenced by the gas velocity, which explains the constant shape of the curve.
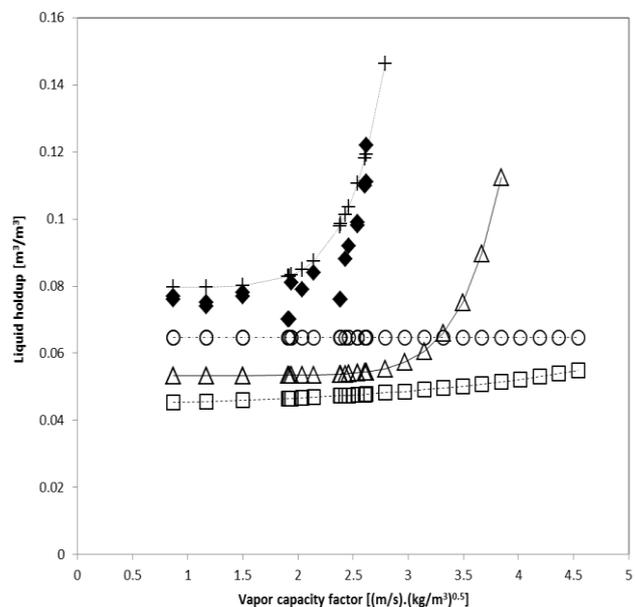

Fig. 4b. Liquid holdup evaluation for liquid load u_L = 20.5 m/h.

Models: (—△—) Billet & Schultes ; (- -□- -) SRP ; (- ·○- ·) Delft ; (···+···) Billet & Schultes modified "Section 5" ; Experimental values: (♦) [12]

The modified Billet and Schultes model shown in Fig. 4 will be presented in section 5.

The average absolute deviations between predictive models (Billet & Schultes, SRP and Delft) and experimental results for pressure drop and liquid holdup are shown in Table 12.

Table 12. Deviation between predictive models and experimental data

Model	Average Absolute Deviation AAD	
	Pressure drop	Liquid holdup
Billet and Schultes	36	35
SRP	41	44
Delft	481	22
Modified Billet and Schultes	6	10

4.2. Effective interfacial area

In a packed column, the gas and the liquid phases are brought into contact and exchange mass and energy across their common interfacial area. The effective interfacial area accounts for the dead area that does not actively take part in the mass transfer process [5].

Fig. 5 shows the results of the effective interfacial area obtained with the three models, and compared to experimental data.
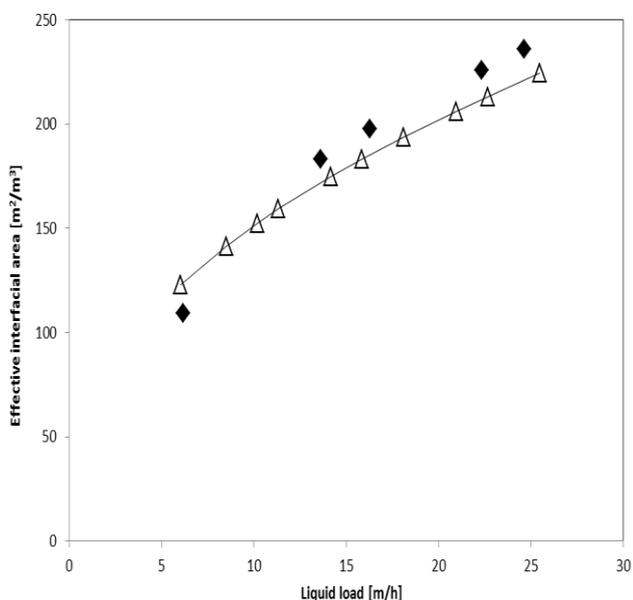
Fig. 5a. Prediction of effective interfacial area by Billet and Schultes model for the system Air / Kerosol 200.

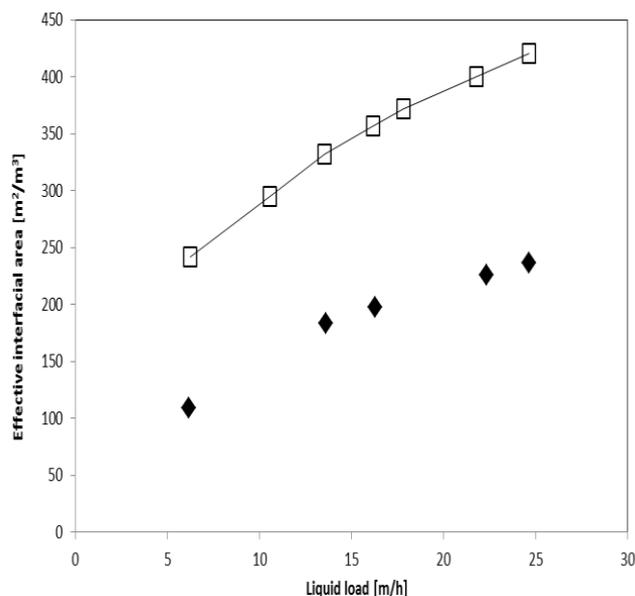Models: (——Δ——) Billet & Schultes ; (♦) Experimental values [12]

Fig. 5b. Prediction of effective interfacial area by SRP model for the system Air / Kerosol 200.

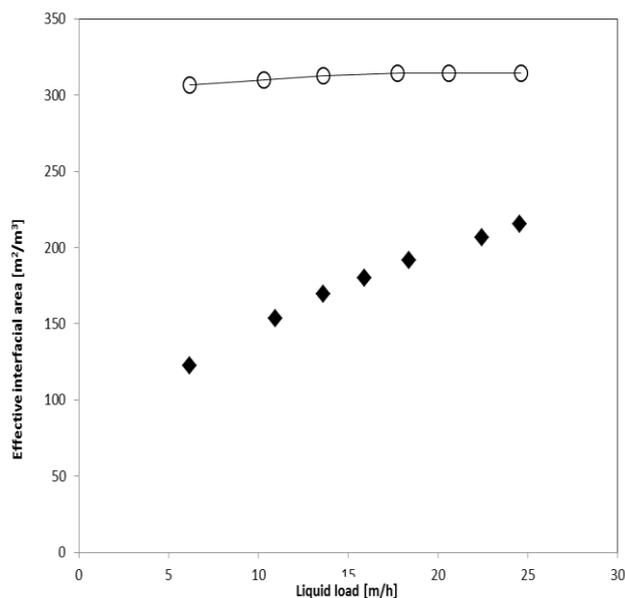Models: (——□——) SRP ; (♦) Experimental values [12]

Fig. 5c. Prediction of effective interfacial area by Delft model for the system Air / Kerosol 200.

Models: (——○——) Delft ; (♦) Experimental values [12]

Fig. 5 shows that most models overpredict the effective interfacial area.

The Delft model assumes that the liquid load does not influence the effective interfacial area which presents 90 % of the overall specific area of Flexipac 350 Y as seen in Fig. 5c.

Compared to the Delft model, the SRP model predicts the right slope of the curve. However, for liquid loads above 16 m/h, the predicted effective interfacial area becomes larger than the packing specific surface.

The Billet and Schultes model is accurate in predicting the effective interfacial area.

The evaluation of the three models shows that the Billet and Schultes model predicts hydrodynamic parameters more accurately than SRP and Delft models. Therefore, the model by Billet and Schultes is retained for the further study.

5. Changes made to Billet and Schultes model and results

The Billet and Schultes model was developed for random packings and then it was extended to cover a limited number of commercially available structured packings.

To make this model more realistic and more accurate in predicting hydrodynamic parameters for structured packings, some constants and exponents defined according to experimental observations and used in the correlations were modified as function of liquid load and density. The constants and exponents to modify were selected following a sensitivity analysis. The values of the constants and exponents have been optimized by minimization of an objective function based on the deviations between modelling and experimental results. The modifications made to equations (15), (20), (27) and (28) are shown in Tables 13, 14 and 15 for liquid holdup and pressure drop. These equations are reminded below by highlighting the modified constants.

$$h_{L,pl} = C_1 \left(\frac{\mu_L \, a^2 \, u_L}{\rho_L \, g} \right)^{\frac{1}{3}} \left(\frac{a_h}{a} \right)^{\frac{2}{3}} \tag{63}$$

$$h_L = h_{L,pl} + \left(C_2 \, h_{L,Fl} - h_{L,pl} \right) \left(\frac{u_V}{u_{V,Fl}} \right)^{n_1} \tag{64}$$

$$\psi_L' = \psi_L \, f_w = C_p \left(\frac{h_L}{h_{L,lp}} \right)^{n_2} \exp \left(\frac{Re_L}{200} \right) \left(\frac{64}{Re_V} + \frac{1,8}{Re_V^{0,08}} \right) \left(\frac{\varepsilon - h_L}{\varepsilon} \right)^{n_3} \tag{65}$$

$$\frac{dP}{dz} = C_3 \, \psi_L \, \frac{f_w \, a}{(\varepsilon - h_L)^3} \frac{F_c^2}{2} \frac{1}{K} \tag{66}$$

In order to improve predictions, equations (15), (20), (27) and (28) were slightly modified based on the experimental results of Erasmus [12], but using only three values of liquid load (u_L = 6 m/h, u_L = 20.5 m/h and u_L = 35.5 m/h) for regression set. The modifications made to equations are coloured in red.

Table 13. Changes made to Billet and Schultes model to calculate liquid holdup

Equations to modify	New equations
(63)	For liquid density > 900 kg/m3 $$h_{L,pl} = [628.4 * (u_L * 3600)^{-0.929}]^{\frac{1}{3}} \left(\frac{\mu_L \, a^2 \, u_L}{\rho_L \, g} \right)^{\frac{1}{3}} \left(\frac{a_h}{a} \right)^{\frac{2}{3}}$$
	For liquid density ≤ 900 kg/m3 $$h_{L,pl} = Exp(-0.0057 * u_L * 3600 + 1.2074) \left(\frac{\mu_L \, a^2 \, u_L}{\rho_L \, g} \right)^{\frac{1}{3}} \left(\frac{a_h}{a} \right)^{\frac{2}{3}}$$
(64)	For liquid density > 900 kg/m3 $$h_{L,pl} = Exp(-0.0057 * u_L * 3600 + 1.2074) \left(\frac{\mu_L \, a^2 \, u_L}{\rho_L \, g} \right)^{\frac{1}{3}} \left(\frac{a_h}{a} \right)^{\frac{2}{3}}$$

	For liquid density $\leq$ 900 kg/m3
	$h_L = h_{L,pl} + \left(Exp\left[-0.0006 * (u_L * 3600)^2 - 0.031 * u_L * 3600 + 0.3736\right] * h_{L,Fl} \right.$ $\left. - h_{L,pl}\right)\left(\frac{u_V}{u_{V,Fl}}\right)^{[-0.0215 * (u_L * 3600)^2 + 0.8927 * u_L * 3600 + 5.3358]}$

Table 14. Changes made to Billet and Schultes model to calculate pressure drop for liquid density lower than 900 kg/m^3

Equations to modify	New equations
(65)	**Preloading region** $$\psi'_L = \psi_L f_w = C_p \left(\frac{h_L}{h_{L,lp}}\right)^{0.3} \exp\left(\frac{Re_L}{200}\right)\left(\frac{64}{Re_V} + \frac{1,8}{Re_V^{0,08}}\right)\left(\frac{\varepsilon - h_L}{\varepsilon}\right)^{1.5}$$ **Loading & Flooding regions** $$\psi'_L = \psi_L f_w = C_p \left(\frac{h_L}{h_{L,lp}}\right)^{0.6} \exp\left(\frac{Re_L}{200}\right)\left(\frac{64}{Re_V} + \frac{1,8}{Re_V^{0,08}}\right)\left(\frac{\varepsilon - h_L}{\varepsilon}\right)^{0.5}$$
(66)	**Preloading region** $$\frac{dP}{dz} = Exp\left(0.0149 * u_L * 3600 + 0.0829\right) \psi_L \frac{f_w a}{(\varepsilon - h_L)^3} \frac{F_c^2}{2} \frac{1}{K}$$ **Loading & Flooding regions** $$\frac{dP}{dz} = 0.002 * (u_L * 3600)^2 - 0.0534 * u_L + 1.76 \, \psi_L \frac{f_w a}{(\varepsilon - h_L)^3} \frac{F_c^2}{2} \frac{1}{K}$$

Table 15. Changes made to Billet and Schultes model to calculate pressure drop for liquid density higher than 900 kg/m^3

Equation to modify	New equations
(65)	**Preloading region** $$\psi'_L = \psi_L f_w = C_p \left(\frac{h_L}{h_{L,lp}}\right)^{0.3} \exp\left(\frac{Re_L}{200}\right)\left(\frac{64}{Re_V} + \frac{1,8}{Re_V^{0,08}}\right)\left(\frac{\varepsilon - h_L}{\varepsilon}\right)^{1.5}$$ **Loading region (For $h_L > h_{L,lp}$)** $$\psi'_L = \psi_L f_w = C_p \left(\frac{h_L}{h_{L,lp}}\right)^{5} \exp\left(\frac{Re_L}{200}\right)\left(\frac{64}{Re_V} + \frac{1,8}{Re_V^{0,08}}\right)\left(\frac{\varepsilon - h_L}{\varepsilon}\right)^{12}$$ **Loading region (For $h_L \leq h_{L,lp}$)** $$\psi'_L = \psi_L f_w = C_p \left(\frac{h_L}{h_{L,lp}}\right)^{0.3} \exp\left(\frac{Re_L}{200}\right)\left(\frac{64}{Re_V} + \frac{1,8}{Re_V^{0,08}}\right)\left(\frac{\varepsilon - h_L}{\varepsilon}\right)^{3}$$

(66)	Flooding region $$\psi_L' = \psi_L\, f_w = C_p \left(\frac{h_L}{h_{L,lp}}\right)^{0.6} \exp\left(\frac{Re_L}{200}\right) \left(\frac{64}{Re_V} + \frac{1.8}{Re_V^{0.08}}\right) \left(\frac{\varepsilon - h_L}{\varepsilon}\right)^{1.5}$$
	Preloading region $$\frac{dP}{dz} = 1.2\, \psi_L\, \frac{f_w\, a}{(\varepsilon - h_L)^3}\, \frac{F_c^2}{2}\, \frac{1}{K}$$
	Loading region $$\frac{dP}{dz} = 1.5\, \psi_L\, \frac{f_w\, a}{(\varepsilon - h_L)^3}\, \frac{F_c^2}{2}\, \frac{1}{K}$$
	Flooding region $$\frac{dP}{dz} = 1.4\, \psi_L\, \frac{f_w\, a}{(\varepsilon - h_L)^3}\, \frac{F_c^2}{2}\, \frac{1}{K}$$

The refined model is then compared to an extended range of experimental data retrieved also from the work of Erasmus [12] in order to validate the new model.

Comparisons to validate the modified model were made at various liquid loads and using two different systems: Air – Water and Air – Kerosol 200. Results of liquid holdup and pressure drop of the two systems over Flexipac 350Y are presented in Fig. 6 and 7.

The same conditions used to evaluate the three models (Type of packing: Flexipac 350Y, system: Air – Water, Pressure drop

Liquid load: 20.5 m/h) are used again in order to evaluate the new model and compare it to the other ones and to the experimental data. In Fig. 4, the experimentally determined pressure drop and liquid holdup [12] are compared to the results obtained with all the models including the new one.

Table 12 presents the deviations between predictive models (Billet & Schultes, SRP and Delft), the modified Billet and Schultes model and experimental results for pressure drop and liquid holdup.
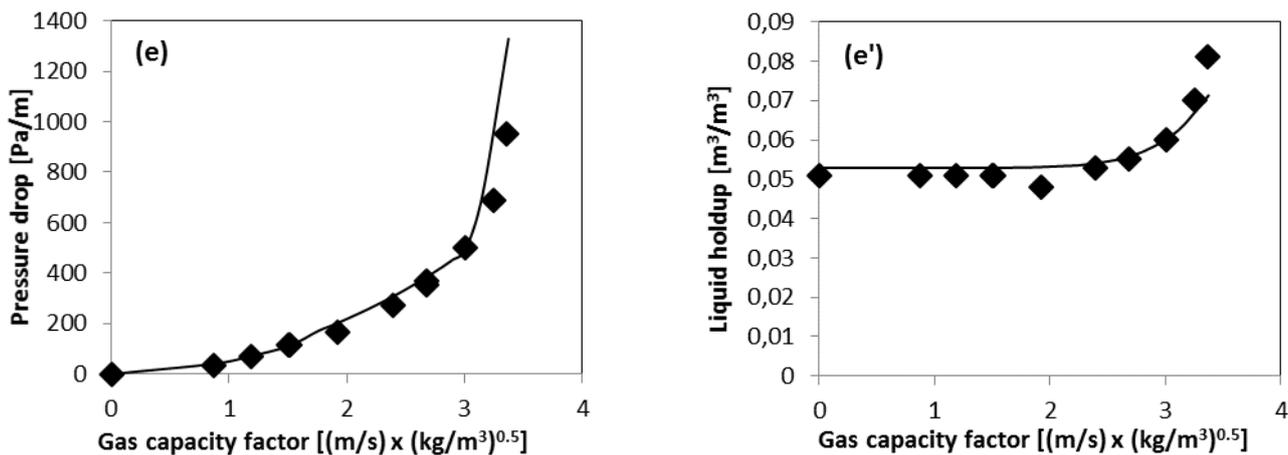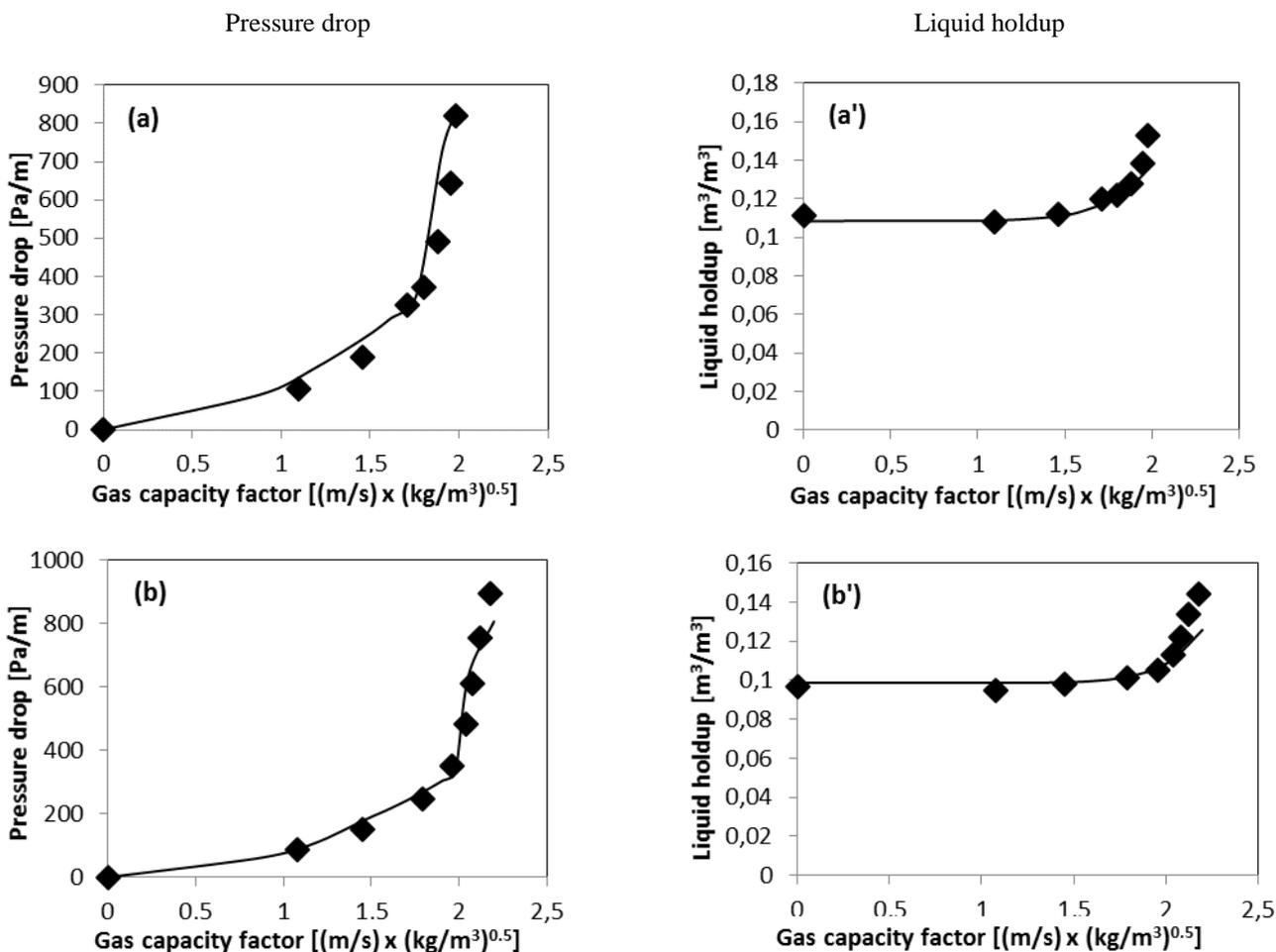
Pressure drop
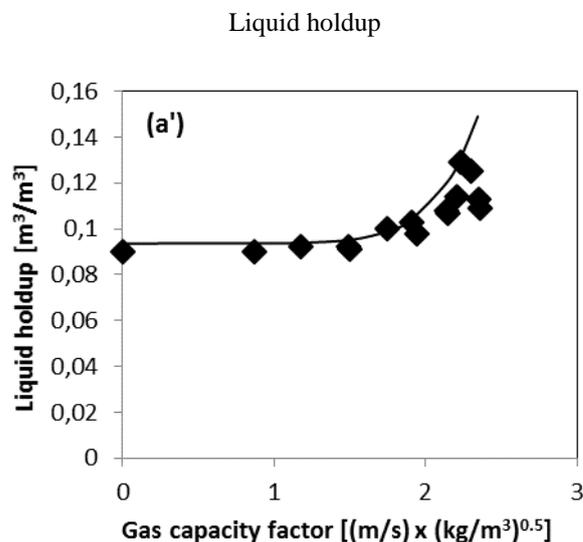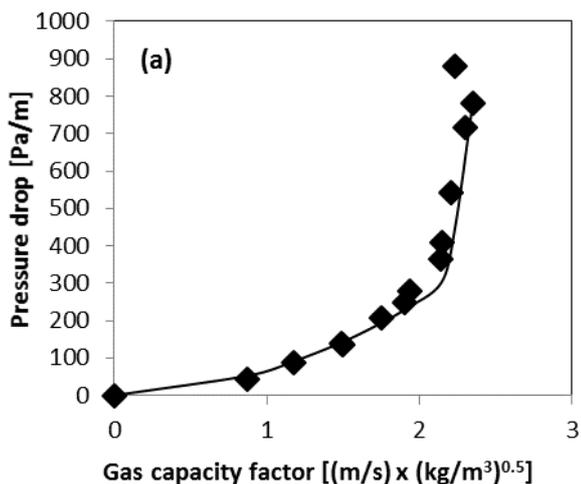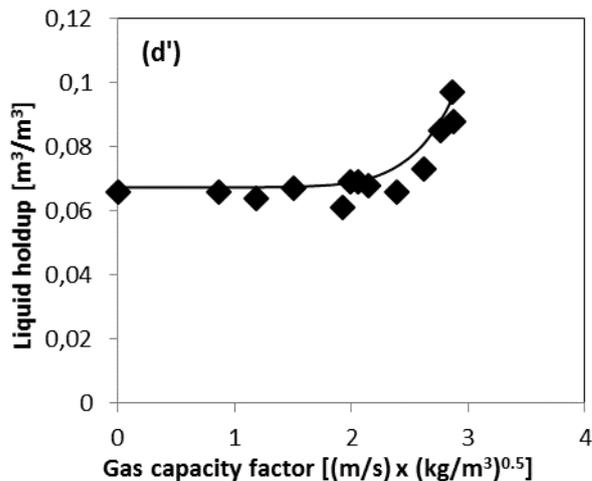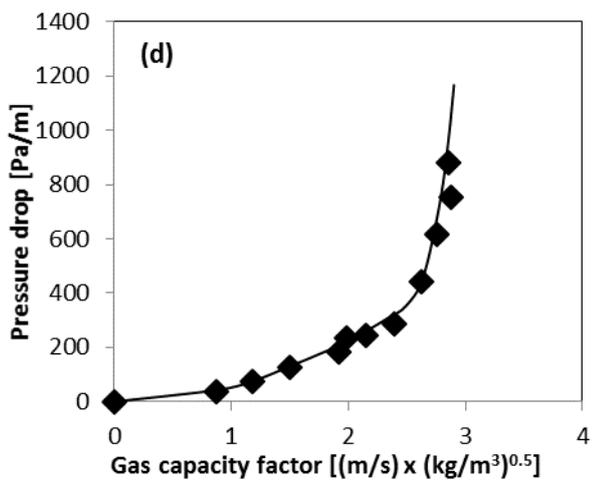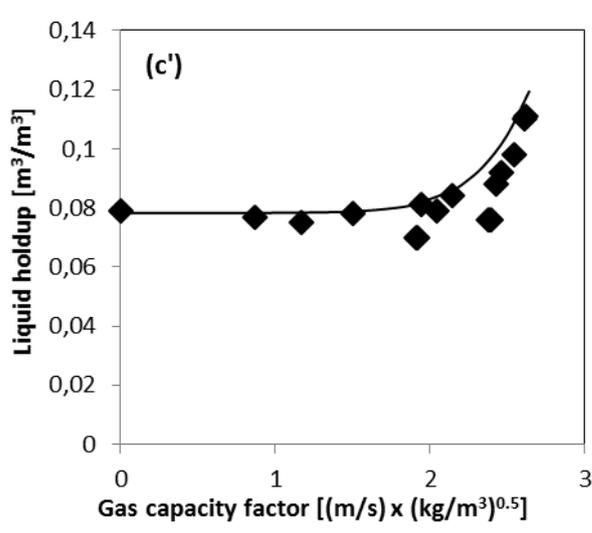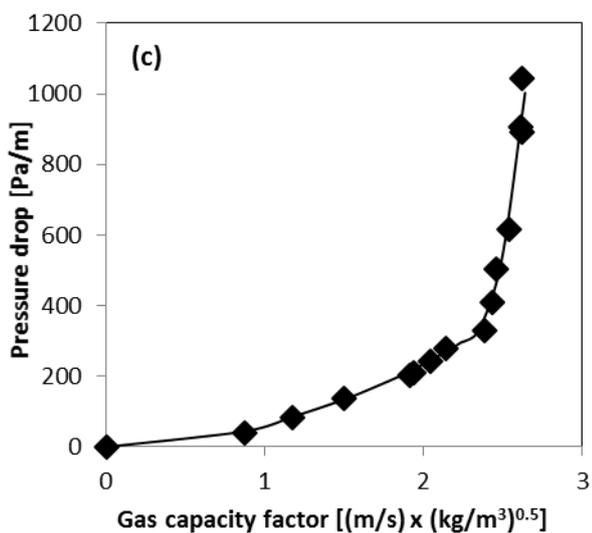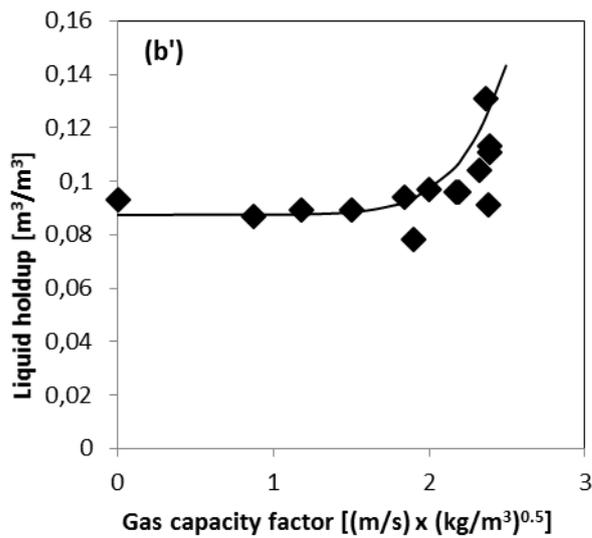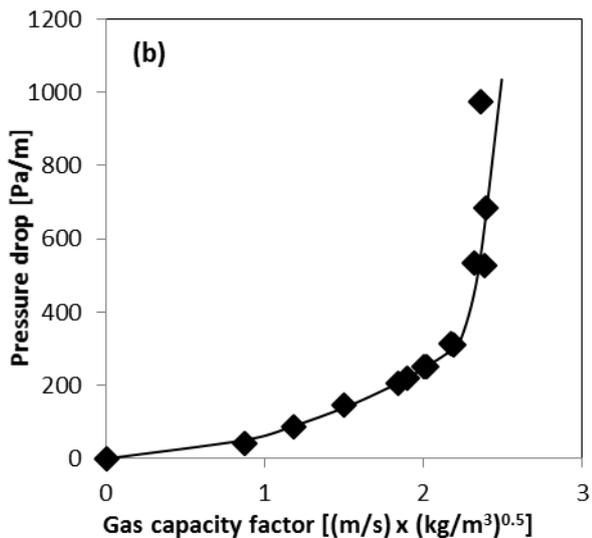
Liquid holdup

Fig. 6. Liquid holdup and pressure drop with an Air – Water system using Flexipac 350Y packing.

Models: (—) Billet & Schultes modified ; (♦) Experimental values [12]
Liquid loads: (a), (a') u_L = 35.6 m/h ; (b), (b') u_L = 28.8 m/h ; (c), (c') u_L = 20.5 m/h ; (d), (d') u_L = 12.9 m/h ; (e), (e') u_L = 6 m/h

Pressure drop   Liquid holdup
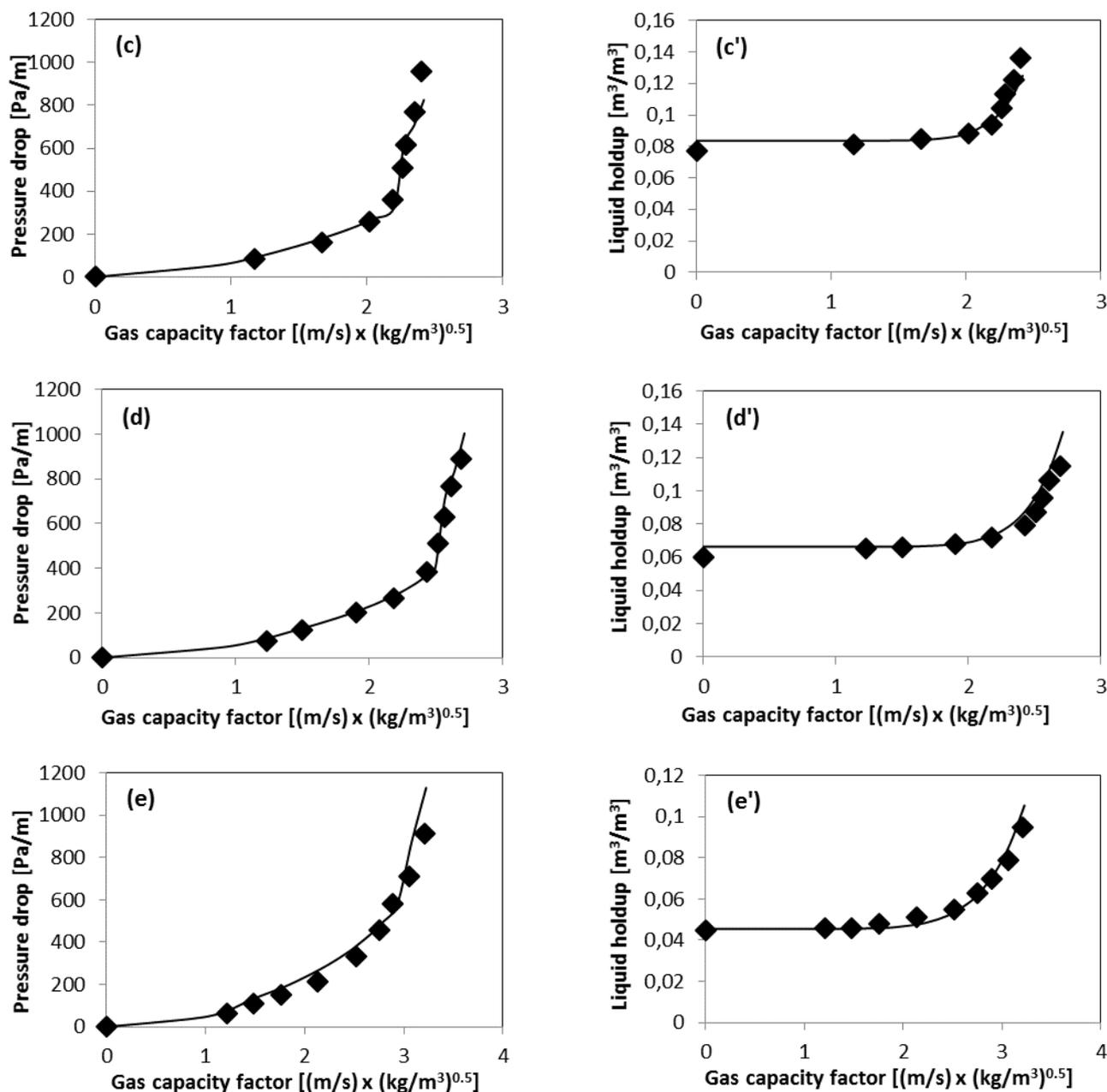
Fig. 7. Liquid holdup and pressure drop with an Air – Kerosol 200 system using Flexipac 350Y packing.

Models: (—) Billet & Schultes modified ; (♦) Experimental values [12]

Liquid loads: (a), (a') u_L = 35.6 m/h ; (b), (b') u_L = 28.8 m/h ; (c), (c') u_L = 20.6 m/h ; (d), (d') u_L = 12.7 m/h ; (e), (e') u_L = 6.1 m/h

Statistical deviation between experimental data and the modified model results are presented in Table 16 for both systems.

Table 16. Statistical deviation between the modified model and experimental data for pressure drop and liquid holdup predictions

Air / Water System				
Liquid load [m/h]	Pressure drop		Liquid holdup	
	AAD [%]	MAD [%]	AAD [%]	MAD [%]

35.6	10	19	7	11
28.8	5	22	2	6
20.5	5	18	6	16
12.9	8	22	4	12
6	9	21	7	12

Air / Kerosol 200 System				
Liquid load [m/h]	Pressure drop		Liquid holdup	
	AAD [%]	MAD [%]	AAD [%]	MAD [%]
35.6	9	26	3	11
28.8	7	20	3	12

20.6	6	13	4	8
12.7	5	12	6	9
6.1	12	23	4	11

After validation of the modified model, it was used to predict pressure drop on a real structured packing column used for the removal of H_2S from biogas.

The results between experimental data obtained from BioGNVAL pilot plant and the refined model are shown in Table 17. The specific constant C_p for pressure drop over Montz B1-420 packing was set to 0.14 by fitting it on experimental data.
The difference between the two results could be explained by pressure drop in the piping which does not contain packing.

Table 17. Comparison between modified correlations and experimental data for the prediction of pressure drop in a structured packing column

No. of point	L [kg/h]	V [kg/h]	$(\Delta P)_{exp}$ [Pa]	$(\Delta P)_{modified\ model}$ [Pa]	$(\Delta P)_{original\ model}$ [Pa]	Absolute value of relative deviation between experimental and modified model [%]	Absolute value of relative deviation between experimental and original model [%]
1	818	89.7	304.4	289.5	200.0	4.89	34.29
2	809	90.2	310.4	292.2	201.6	5.88	35.07
3	809	90.9	312.3	296.5	204.3	5.06	34.58
4	809	91.2	312.4	298.8	205.8	4.36	34.13
5	850	91.8	321.2	307.8	211.1	4.18	34.28
6	854	92.6	325.5	313.3	214.5	3.74	34.09
7	870	93.0	323.9	318.6	217.6	1.63	32.81
8	821	93.8	325.6	318.0	217.7	2.33	33.13
9	797	94.9	326.2	322.6	220.8	1.10	32.31
10	855	95.4	345.0	334.0	227.1	3.16	34.15

6. Conclusion

This study evaluated three semi-empirical models for prediction of hydrodynamic parameters used for an industrial application concerning biogas purification: Billet and Schultes, SRP and Delft.

Flexipac 350Y structured packing was considered here. Its capacity is closely related to hydrodynamics and mass transfer characteristics. That is why, the performances of these hydrodynamic models were investigated and compared based on existing experimental data, and the choice was finally made on the model of Billet and Schultes.

The correlations of this model were improved in order to develop an accurate prediction of hydrodynamic parameters in a structured packing column.
This model allows to precisely predicting the key hydrodynamic parameters: liquid holdup, pressure drop, effective interfacial area and especially the two transition points: loading and flooding points.

The results of pressure drop using the modified model were compared to those obtained on the BioGNVAL pilot plant treating 85 Nm^3/h of biogas. Good agreement was obtained with experimental data.

It is wise to note that this model may lose generality with varying applications but for the activities of interest, it wins precision. Therefore, this modified model is ideal to predict accurately the three operating regions of a small scale structured packing column used for biogas or natural gas applications. It would allow the design of structured packing columns without the need of experimental data collected on a pilot plant. The operative conditions of the existing columns could also be optimized using the modified model to operate at full capacity.

References

[1] Strigle, R. F. Jr., 1994, "Packed tower design and applications, Random and structured packings, second edition.".

[2] EIGA Publication AHG IGC 1.1. Carbon Dioxide Source Certification, Qualify Standards and Verification. European Industrial Gases Association. 1999.

[3] www.cryopur.com (Cryo Pur® company), 25/07/2016.

[4] Chan, H. and Fair, J. R., 1983, "Industrial and Engineering Chemistry Process Design and Development." 23-814.

[5] Paquet, E. F., 2011, "Establishing a facility to measure the efficiency of structured packing under total reflux." MSc, Stellenbosch: University of Stellenbosch.

[6] Schultes, M., 2010. "Research on mass transfer columns "Old hat or still relevant ?"." Distillation Absorption, Eindhoven, the Netherlands, 37-42.

[7] Billet, R. and Schultes, M., 1993. "A physical model for the prediction of liquid hold-up in two-phase counter-current columns." Chemical Engineering & Technology, 16:370-375.

[8] Bravo, J. L., Rocha, J. A. and Fair, J. R., 2000, "A comprehensive model for the performance of columns containing structured packings." Institution of Chemical Engineers Symposium Series 128, Birmingham, 1:A489-A507.

[9] Olujić, Ž., Behrens, M., Colli, L. and Paglianti, A., 2004, "Predicting the efficiency of corrugated sheet structured packings with large specific surface area." Chemical and Biochemical Engineering Quarterly 18:89-96.

[10] Billet, R. and Schultes, M., 1999, "Prediction of mass transfer columns with dumped and arranged packings: Updated summary of the calculation method of Billet and Schultes." Chemical Engineering Research and Design 77:498-504.

[11] Lamprecht, S. M., 2010. "Establishing a facility to measure packed column hydrodynamics." MSc, Stellenbosch: University of Stellenbosch.

[12] Erasmus, A. B., 2004, "Mass transfer in structured packing." Thesis, Departement of Process Engineering at the University of Stellenbosch.

[13] Gualito, J. J., Cerino, F. J., Cardenas, J. C. and Rocha, J. A., 1997, "Design method for distillation columns filled with metallic, ceramic, or plastic structured packings." Industrial & Engineering Chemistry Research 36:1747-1757.